

## LOW ENERGY ANTIKAON-NUCLEON/NUCLEI INTERACTION STUDIES BY AMADEUS\*

K. PISCICCHIA<sup>a,b</sup>, M. CARGNELLI<sup>c</sup>, C. CURCEANU<sup>b</sup>, R. DEL GRANDE<sup>b</sup>  
 L. FABBIETTI<sup>d,e</sup>, C. GUARALDO<sup>b</sup>, J. MARTON<sup>c</sup>, P. MOSKAL<sup>f</sup>  
 A. SCORDO<sup>b</sup>, M. SILARSKI<sup>f</sup>, D. SIRGHI<sup>b,g</sup>, M. SKURZOK<sup>f</sup>  
 I. TUCAKOVIC<sup>h</sup>, O. VAZQUEZ DOCE<sup>d,e</sup>, S. WYCECH<sup>i</sup>, E. WIDMANN<sup>c</sup>  
 J. ZMESKAL<sup>c</sup>

<sup>a</sup>CENTRO FERMI — Museo Storico della Fisica e Centro Studi e Ricerche  
 “Enrico Fermi”, Roma, Italy

<sup>b</sup>INFN Laboratori Nazionali di Frascati, Frascati (Roma), Italy

<sup>c</sup>Stefan-Meyer-Institut für subatomare Physik, Vienna, Austria

<sup>d</sup>Excellence Cluster “Origin and Structure of the Universe”  
 85748 Garching, Germany

<sup>e</sup>Physik Department E12, Technische Universität München  
 85748 Garching, Germany

<sup>f</sup>M. Smoluchowski Institute of Physics, Jagiellonian University, Kraków, Poland

<sup>g</sup>Horia Hulubei National Institute of Physics and Nuclear Engineering  
 (IFIN-HH), Măgurele, Romania

<sup>h</sup>Ruder Bošković Institute, Zagreb, Croatia

<sup>i</sup>National Centre for Nuclear Research, Warszawa, Poland

*(Received July 3, 2018)*

The AMADEUS experiment at the DAΦNE collider of LNF-INFN deals with the investigation of the at-rest, or low-momentum,  $K^-$  interactions in light nuclear targets, with the aim to constrain the low energy QCD models in the strangeness sector. The 0 step of the experiment consisted in the reanalysis of the 2004/2005 KLOE data, exploiting  $K^-$  absorptions in H,  $^4\text{He}$ ,  $^9\text{Be}$  and  $^{12}\text{C}$ , leading to the first invariant mass spectroscopic study with very low momentum (about 100 MeV) in-flight  $K^-$  captures. With AMADEUS step 1, a dedicated pure carbon target was implemented in the central region of the KLOE detector, providing a high statistic sample of pure at-rest  $K^-$  nuclear interaction. The first measurement of the non-resonant transition amplitude  $|A_{K^-n \rightarrow \Lambda\pi^-}|$  at  $\sqrt{s} = 33$  MeV below the  $\bar{K}N$  threshold is presented, in relation with the  $\Lambda(1405)$  properties studies.

DOI:10.5506/APhysPolBSupp.11.609

---

\* Presented at “Excited QCD 2018”, Kopaonik, Serbia, March 11–15, 2018.

## 1. Introduction

The absorption of low momentum  $K^-$  mesons ( $p_K \sim 127$  MeV/c), produced by the DAΦNE [1] collider, on He and C nuclear targets is investigated, with the aim to get information on the resonant and non-resonant transition amplitudes few MeV below the  $\bar{K}N$  threshold, which represent good tests for the theoretical predictions of the low energy QCD models in the strangeness sector.

The detailed characterisation of the yield and spectral shape of the non-resonant antikaon–nucleon absorption, resulting in a hyperon–pion final state below the  $\bar{K}N$  threshold, is also a fundamental reference to extract the  $\Lambda(1405)$  (isospin  $I = 0$ ) properties in  $\bar{K}N$  absorption experiments from the competing non-resonant  $(\Sigma\pi)^0$  formation. According to the chiral unitary model [2–4] (see also the review [5]), the  $\Lambda(1405)$  can be interpreted as a molecular meson–baryon state, emerging from the interference of two poles, a lower mass pole (about 1390 MeV) which is mainly coupled to the  $\Sigma\pi$  channel and a high mass pole, coupled to the  $\bar{K}N$  production channel, located around 1420 MeV (the next to leading order calculation of the poles masses and widths can be found in [6]). For this reason, the shape of the measured  $(\Sigma\pi)^0$  invariant mass distribution is expected to change depending on the decay channel, due to the isospin interference term (which contributes with opposite sign to the  $\Sigma^\pm\pi^\mp$  cross sections, and vanishes for  $\Sigma^0\pi^0$ ) but also on the production channel. In this scenario, the  $\bar{K}N$  absorption represents the golden channel for investigating the predicted high mass pole of the  $\Lambda(1405)$ .

The capture of  $K^-$  mesons on light nuclear targets (He and C) at-rest was observed in old bubble chamber and emulsion experiments [7–12], where a high purity sample was analysed at the price of a limited statistics. In the case of interactions at-rest, the underlying mechanism consists in the capture of the strange meson in a highly excited atomic state and a successive cascade to low-lying states, followed by the  $K^-$  nuclear capture. Besides the interactions at-rest, an important contribution from in-flight  $K^-$  nuclear captures was already characterised by the AMADEUS Collaboration in previous works [13, 14], using a data sample collected by the KLOE Collaboration in 2004/2005 [15]. The in-flight capture process consists in the kaon propagation through the electron cloud, followed by the nuclear absorption. We will show how the in-flight  $K^-$  absorption on He and C is the optimal production mechanism for the search of the  $\Lambda(1405)$  high mass pole.

## 2. Data samples

The ongoing AMADEUS analyses refer to two data samples. One is represented by the data collected by the KLOE Collaboration during the 2004/2005 data taking, corresponding to  $\sim 1.74$  fb $^{-1}$ . The KLOE detec-

tor [16] is used as an active target, the hadronic interaction of negative kaons with the materials of the apparatus being investigated; in particular  $K^-$ <sup>9</sup>Be absorptions in the DAΦNE beryllium thin cylindrical layer and the DAΦNE aluminated beryllium pipe,  $K^-$ <sup>12</sup>C and  $K^-$ H absorptions in the KLOE Drift Chamber [17] (DC) inner wall (aluminated carbon fibre),  $K^-$ <sup>4</sup>He in the DC gas, filled with a mixture of helium and isobutane (in volume: 90% <sup>4</sup>He and 10% C<sub>4</sub>H<sub>10</sub>). Extremely rich experimental information is contained in this sample, with  $K^-$  hadronic captures both at-rest and in-flight.

In order to increase the statistics and as an essential interpretation tool, a high purity carbon target (graphite) was realized in summer 2012 and installed inside the KLOE detector, between the beam pipe and the DC inner wall. The geometry of the target was optimized to maximize the kaon stopping power (technical details can be found in Ref. [13]). The total collected integrated luminosity is  $\sim 90 \text{ pb}^{-1}$ . Up to now, we analysed a sample of  $37 \text{ pb}^{-1}$  reconstructed data.

Details on the events selection and particle identification for the channels under investigation are given in Ref. [13].

### 3. Resonant and non-resonant $Y\pi$ transition amplitudes below the $\bar{K}N$ threshold

The investigation of the  $\Lambda(1405)$  properties in  $K^-$ -induced reactions on light nuclear targets is strongly biased by the kinematic threshold determined by the absorbing nucleon binding energy. For  $K^-$  captures at-rest on <sup>4</sup>He and <sup>12</sup>C, the  $m_{\Sigma\pi}$  invariant mass thresholds are about 1412 MeV and 1416 MeV respectively. The  $\bar{K}N$  sub-threshold region can be accessed in  $K^-$  in-flight captures by exploiting the negative kaon kinetic energy contribution. For kaon momenta of 100 MeV/c, the  $m_{\Sigma\pi}$  threshold is shifted upwards of about 10 MeV, thus opening the mass window where the high mass pole is predicted.

In Fig. 1 (black distribution), the  $\Sigma^0\pi^0$  invariant mass spectrum from  $K^-$  captures in the KLOE DC wall is shown [18].  $\Sigma^0\pi^0$  represents the best signature of the  $\Lambda(1405)$  resonance, since does not contain isospin  $I = 1$  background. The  $m_{\Sigma 0\pi 0}$  spectrum is compared with the corresponding distribution of  $K^-$  captures at-rest in the pure carbon target (Fig. 1 grey/blue distribution), the grey/blue and the black distributions are normalized to unity. In Fig. 1, a thin black (red) line indicates the energy threshold corresponding to  $K^-$  absorption in <sup>12</sup>C at-rest. A rich sample of in-flight  $K^-$ <sup>12</sup>C captures can be easily identified above the thin black (red) line. The  $\Lambda(1405)$  shape can be now extracted after subtracting the  $\Sigma^0\pi^0$  non-resonant contribution.

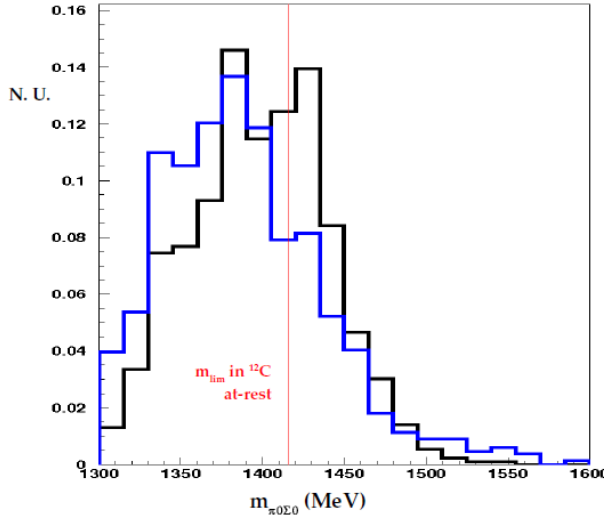


Fig. 1. (Colour on-line)  $m_{\Sigma^0 \pi^0}$  invariant mass distribution from  $K^-$  captures in the KLOE DC wall (black curve) and pure carbon graphite target (grey/blue curve).

In Refs. [19] and [20], the real and imaginary parts of the non-resonant coupled channels  $K^- n \rightarrow \Lambda \pi / \Sigma \pi$  scattering amplitudes, calculated on the basis of several chiral SU(3) meson–baryon coupled channels interaction models (Prague (P) [21], Kyoto–Munich (KM) [6], Murcia (M1,M2) [22] Bonn (B2,B4) [23]) are compared. The amplitudes values strongly differ in the  $\bar{K}N$  sub-threshold region depending on the adopted model.

In order to pin down the model to be adopted for the description of the observed  $\Sigma^0 \pi^0$  spectra, the  $K^- n \rightarrow \Lambda \pi^-$  transition was measured by exploiting  $K^- n$  single nucleon absorptions in  ${}^4\text{He}$ . Since the  $\Sigma^-(1385)$  (isospin  $I = 1$ ) resonance is well-known, the corresponding non-resonant transition amplitude ( $|A_{K^- n \rightarrow \Lambda \pi^-}|$ ) can be extracted and used to test the chiral predictions below threshold. The production of  $\Lambda \pi^-$  pairs in the final state can occur either via direct non-resonant/resonant processes, or via the primary production of a  $\Sigma$ , followed by inelastic Final State Interaction (FSI) of the hyperon. The contribution of the conversion mechanism was minimised by selecting, in the  $p_{\pi^-}$  vs.  $p_\Lambda$  scatterplot, the phase-space region which is populated by the correlated direct  $\Lambda \pi^-$  production. The phase-space cut was optimised based on MC simulations (performed with the standard KLOE GEANT digitization (GEANFI [17])) of all the involved physical processes, according to the calculations reported in [24]. Besides inelastic FSI processes, also elastic FSI processes can occur, namely the re-scattering of the  $\Lambda$  or the  $\pi^-$  on residual nuclear fragments. In [24], the correction to the

amplitude modulus due to these contributions is found to be less than 3% of the total  $K^- n \rightarrow \Lambda\pi^-$  amplitude modulus. For this reason, the elastic FSI contribution is neglected in this analysis.

Since the selected sample of 3050  $\Lambda\pi^-$  events still contains not only direct processes, but also a small contamination of conversion processes, both are simulated and used to fit the experimental distributions in order to extract the amplitude of direct non-resonant processes.

In order to extract the ratio of the resonant over non-resonant  $\Lambda\pi^-$  production, the measured  $p_{\Lambda\pi}$ ,  $m_{\Lambda\pi}$  (invariant mass of the hyperon–pion pair) and  $\cos(\theta_{\Lambda\pi})$  ( $\theta_{\Lambda\pi}$  is the angle between the  $\Lambda$  and  $\pi$  momenta) distributions were fitted. The main background is represented by the  $K^- {}^{12}\text{C}$  absorptions due to the isobutane molecules in the DC gas. In order to account for this contribution, an experimental sample of  $K^- {}^{12}\text{C}$  absorptions is used, obtained by selecting kaons interactions in the DC entrance wall. The carbon-sample is selected adopting the same criteria as for the gas sample and was used in the global fit. The modulus of the amplitude of the non-resonant processes, the ratio of the resonant to non-resonant processes, the modulus of the amplitude of the conversions and the contribution of the  $K^-$  captures on carbon are considered as free parameters in the fit.

Panels (a)–(f) in Fig. 2 show  $p_{\Lambda\pi}$ ,  $\cos(\theta_{\Lambda\pi})$ ,  $m_{\Lambda\pi}$  distributions used for the fit and, additionally, the total hyperon–pion kinetic energy  $T_{\Lambda\pi}$ , as well as the moduli of the  $p_\Lambda$  and  $p_\pi$  momenta.

The systematic errors are estimated by varying independently the selection cuts such as to increase or decrease the  $\Lambda\pi^-$  statistics by 15% with respect to the optimized selection. The chi-square of the fit is  $\chi^2/\text{n.d.f.} = 151/148$ . Table I shows the fit results, where the resonant to non-resonant ratios ( $\frac{\text{RES}}{\text{NR}}$ ) for at-rest and in-flight reactions are shown together with the yields of the various channels obtained from the fit.

The ratio ( $\frac{\text{RES-if}}{\text{NR-if}}$ ) for the  $\Lambda\pi^-$  production in-flight is found to be smaller than the corresponding ratio at-rest. This is not surprising as the  $K^- n$  interaction in-flight occurs about  $\sqrt{s} = 20$  MeV below the  $\bar{K}N$  threshold; the corresponding reaction at-rest occurs about  $\sqrt{s} = 33$  MeV below the threshold (see Ref. [24]), nearer to the resonance which lays about 49 MeV below the  $\bar{K}N$  threshold. The systematic uncertainty on the resonant-to-non-resonant ratio for the in-flight reactions prevents from extracting the modulus of the non-resonant transition amplitude in-flight. The corresponding transition amplitude modulus at-rest, extracted by comparing Eq. (14) and Eq. (20) in Ref. [24] with the experimental result ( $\frac{\text{RES-ar}}{\text{NR-ar}}$ ) is:

$$|A_{K^- n \rightarrow \Lambda\pi^-}| = (0.334 \pm 0.018 \text{ stat}^{+0.034}_{-0.058} \text{ syst}) \text{ fm}. \quad (1)$$

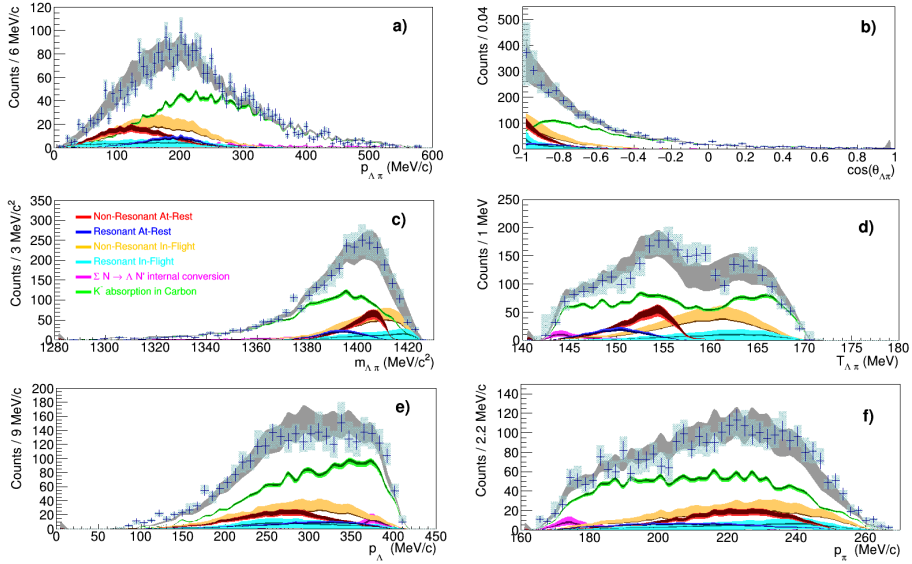


Fig. 2. (Colour on-line) Panels (a)–(f):  $p_{\Lambda\pi}$ ,  $\cos(\theta_{\Lambda\pi})$ ,  $m_{\Lambda\pi}$ ,  $T_{\Lambda\pi}$ ,  $p_{\Lambda}$  and  $p_{\pi}$  distributions. The experimental data and the corresponding statistical errors are represented by the black crosses, the systematic errors are light blue boxes. The different contributions included in the fit are shown by the colored histograms: non-resonant at-rest (red), resonant at-rest (blue), non-resonant in-flight (brown), resonant in-flight (cyan),  $\Sigma N \rightarrow \Lambda N'$  internal conversion (magenta),  $K^-$  absorptions in carbon (green). The light and dark bands correspond to systematic and statistical errors, respectively. The grey band shows the total fit with the corresponding statistical error. See the text for details.

TABLE I

Resonant-to-non-resonant ratios and amplitudes of the various channels extracted from the fit of the  $\Lambda\pi^-$  sample. The statistical and systematic errors are also shown. See the text for details.

Channels	Ratio/yield	$\sigma_{\text{stat}}$	$\sigma_{\text{syst}}$
RES-ar/NR-ar	0.39	$\pm 0.04$	$+0.18$ $-0.07$
RES-if/NR-if	0.23	$\pm 0.03$	$+0.23$ $-0.22$
NR-ar	12.0%	$\pm 1.7\%$	$+2.0\%$ $-2.8\%$
NR-if	19.2%	$\pm 4.4\%$	$+5.9\%$ $-3.3\%$
$\Sigma \rightarrow \Lambda$ conv.	2.2%	$\pm 0.3\%$	$+1.6\%$ $-0.8\%$
$K^-$ $^{12}\text{C}$ capture	57.0%	$\pm 1.2\%$	$+2.2\%$ $-3.2\%$

#### 4. Discussion

In this work, the measurement of the isospin  $I = 1$  non-resonant transition amplitude  $|A_{K^-n \rightarrow \Lambda\pi^-}|$  at  $\sqrt{s} = 33$  MeV below the  $\bar{K}N$  threshold is presented. The result of this analysis (with combined statistical and systematic errors) is shown in Fig. 3 and compared with the theoretical predictions (see Ref: [21] (P), [6] (KM), [22] (M1,M2), [23] (B2,B4)) rescaled for the  $K^-n \rightarrow \Sigma\pi$  transition probabilities. The presented result allows an extrapolation to the un-physical region and can be used to test models of S-wave interaction; moreover, such extrapolation can be used to constrain the corresponding  $(\Sigma\pi)^0$  non-resonant background for the extraction of the  $\Lambda(1405)$  properties in  $\bar{K}N$  absorption experiments.

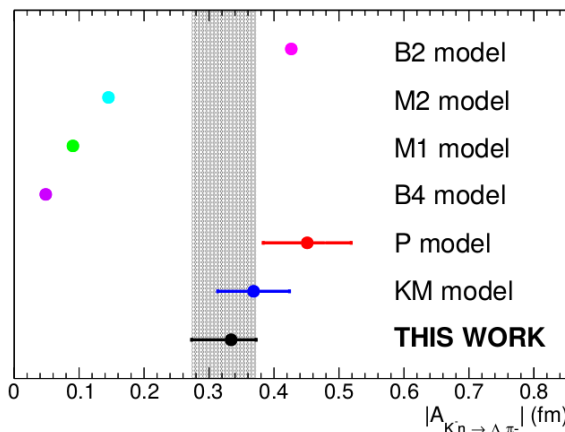


Fig. 3. (Colour on-line) Modulus of the measured non resonant  $K^-n \rightarrow \Lambda\pi^-$  transition amplitude compared with theoretical calculations, see details in the text.

We acknowledge the KLOE/KLOE-2 Collaboration for their support and for having provided us the data and tools to perform the analysis presented in this paper. We acknowledge the CENTRO FERMI — Museo Storico della Fisica e Centro Studi e Ricerche “Enrico Fermi” for the project PAMQ. Part of this work was supported by the Austrian Science Fund (FWF): [P24756-N20]; Austrian Federal Ministry of Science and Research BMBWK 650962/0001 VI/2/2009; the Croatian Science Foundation, under project 1680; Ministero degli Affari Esteri e della Cooperazione Internazionale, Direzione Generale per la Promozione del Sistema Paese (MAECI), Strange Matter project; National Science Center, Poland (NCN) through grant No. UMO-2016/21/D/ST2/01155.

## REFERENCES

- [1] A. Gallo *et al.*, in: Proceedings of 10<sup>th</sup> European Particle Accelerator Conference, EPAC 2006, Edinburgh, United Kingdom, 26–30 June 2006; Code 104533, pp. 604–606.
- [2] J.A. Oller, U.G. Meißner, *Phys. Lett. B* **500**, 263 (2001).
- [3] T. Hyodo *et al.*, *Phys. Rev. C* **68**, 018201 (2003).
- [4] D. Jido *et al.*, *Nucl. Phys. A* **725**, 181 (2003).
- [5] T. Hyodo, D. Jido, *Prog. Part. Nucl. Phys.* **67**, 55 (2012).
- [6] Y. Ikeda, T. Hyodo, W. Weise, *Nucl. Phys. A* **881**, 98 (2012).
- [7] P.A. Katz *et al.*, *Phys. Rev. D* **1**, 1267 (1970).
- [8] K. Brunnel *et al.*, *Phys. Rev. D* **2**, 98 (1970).
- [9] D. Riley *et al.*, *Phys. Rev. D* **11**, 3065 (1975).
- [10] Proceedings of the International Conference on Hypernuclear Physics, Argonne National Laboratory, USA, May 5–7, 1969.
- [11] P.J. Carlson *et al.*, *Nucl. Phys.* **74**, 642 (1965).
- [12] A. Barbaro-Galtieri *et al.*, *Phys. Lett. A* **5**, 63 (1963).
- [13] C. Curceanu *et al.*, *Acta Phys. Pol. B* **46**, 203 (2015).
- [14] O. Vazquez Doce *et al.*, *Phys. Lett. B* **758**, 134 (2016).
- [15] F. Bossi [KLOE Collaboration], *Riv. Nuovo Cim.* **31**, 531 (2008).
- [16] F. Ambrosino *et al.*, *Nucl. Instrum. Methods Phys. Res. A* **534**, 403 (2004).
- [17] M. Adinolfi *et al.* [KLOE Collaboration], *Nucl. Instrum. Methods Phys. Res. A* **488**, 51 (2002).
- [18] K. Piscicchia, Ph.D. Thesis, 2013, Lambda(1405) Measurement Through the Decay to  $\Sigma^0\pi^0$ , Resulting from  $K^-$  Meson Absorption on  ${}^4\text{He}$  and  ${}^{12}\text{C}$ , with the KLOE Detector,  
[http://www.infn.it/thesis/thesis\\_dettaglio.php?tid=7097](http://www.infn.it/thesis/thesis_dettaglio.php?tid=7097).
- [19] J. Hrtankova, J. Mares, *Phys. Rev. C* **96**, 015205 (2017).
- [20] A. Cieplý *et al.*, *Nucl. Phys. A* **954**, 17 (2016).
- [21] A. Cieplý, J. Smejkal, *Nucl. Phys. A* **881**, 115 (2012).
- [22] Z.H. Guo, J.A. Oller, *Phys. Rev. C* **87**, 035202 (2013).
- [23] M. Mai, U.G. Meißner, *Eur. Phys. J. A* **51**, 30 (2015).
- [24] K. Piscicchia, S. Wycech, C. Curceanu, *Nucl. Phys. A* **954**, 75 (2016).